Investigation of the inner edge of neutron star crusts: Temperature dependence and related effects

W. M. Seif [1,2,*], A. S. Hashem [1], and Youstina Ramsis [1]

[1]*Cairo University, Faculty of Science, Department of Physics, 12613 Giza, Egypt*
[2]*Cairo University, Faculty of Postgraduate Studies for Nanotechnology, Egypt*

The mutual correlation between the nuclear equation of state (EOS) and the bulk properties of neutron stars (NS) is crucial in probing both of them. Here, we use EOSs of hot npe ($npe\mu$) nuclear matter, based on the density-dependent CDM3Y-Paris nucleon-nucleon interaction in the nonrelativistic Hartree-Fock scheme, to investigate the temperature dependence of the core-crust transition properties under β equilibrium, at the inner edge of NS. We use four EOSs that provide symmetric nuclear matter saturation incompressibility of 218 and 252 MeV, with two parametrizations of the density dependence of the isovector part of the M3Y force. We found that the softer EOS estimates larger proton fraction in the NS matter and indicates a wider range for direct Urca (DU) cooling process within the core center of NSs. Increasing the temperature decreases the density corresponding to the threshold proton fraction for DU process, increasing the region for the DU process inside NSs. The muons decrease the isospin asymmetry of the $npe\mu$ NS matter at its core center, its thermal pressure, and the DU threshold density. The muon fraction slightly changes with temperature. A value of about half the proton fraction is inferred for the β-stable muon fraction of hot $npe\mu$ matter, around the core center. Based on the four considered EOSs, the liquid core-solid crust transition density, pressure, and proton fraction are estimated to increase from $(0.54 \pm 0.02)\rho_0$, 0.36 ± 0.12 MeV fm^{-3}, and 0.03, respectively at $T = 0$ MeV, to $(0.85 \pm 0.04)\rho_0$, 7.36 ± 0.52 MeV fm^{-3}, and 0.14, respectively at $T = 50$ MeV.

I. INTRODUCTION

Over the past decades, neutron stars (NS) had a significant importance in physics and astrophysics, as a rich physical system. Their importance stem from the wealthy structure of their matter under extreme physical conditions [1]. NS form the remains of massive stars when their lives end in supernova explosions [2]. They result from the gravitational collapse of an ordinary star with a large mass ranging from 8 to $25M_\odot$ in a supernova event, with temperature reaches several tens of MeV [2]. The supernova explosion [3–6] happens when the star exhausts its fuel by nuclear fusion. The star then becomes unstable and collapses due to the insufficient pressure gradient provided by the radiation to balance the gravitational attraction [1,2,7]. Consequently, the temperature cools down by neutrino emission within the first minute. While the temperatures in the cores of the compact stars are low relative to the Fermi energy, the density increases up to ten times the saturation nuclear density (ρ_0). A temperature of more than 50 MeV can be reached for hot proto-neutron star (PNS) [8,9] formed in the supernova explosion. Higher temperatures of about 100 MeV can be attained in the neutron-star binary systems [7]. The structure of the neutron stars can be divided into atmosphere and four internal regions, namely the inner and the outer crust and the inner and the outer core [1,2,7]. The atmosphere [10,11] takes shape of a thin layer of plasma with a thickness varies from tens of centimeters in hot NS

to a few millimeters in a cold one. The outer crust consists of ions and electrons, over a thickness of about hundreds of meters. Going deeper in the neutron star, the density increases and so the electron Fermi energy, which induces β captures and enriches nuclei with neutrons. The inner crust consists of free neutrons, neutron rich nuclei and electrons. Its thickness is about one kilometer and the density reaches about $0.5\rho_0$ at its base. The outer core consists of neutrons with admixture of electrons, protons and possible muons, with a thickness extends to several kilometers. The corresponding density varies from $0.5\rho_0$ to about $2\rho_0$. An ideal Fermi gas is formed by electrons and muons. The inner core occupies the center of massive neutron and proto-neutron stars; with a radius of several kilometers and central density exceeds 1 fm^{-3} and even reaches $(10–15)\rho_0$ [12–15]. Different models have been used to describe the composition and the related EOS of the inner core. The EOSs adopted in the present study success to describe the dense NM up to such compact densities [16,17].

The composition of NS, which varies from pure neutron matter (PNM) to symmetric matter (SNM), is determined by equilibrium condition and charge neutrality with respect to weak interaction. The matter of NS maintains beta equilibrium, $n \rightarrow p + e^- + \tilde{\nu}_e$ [18,19]. As the density increases, and with the chemical potential of electron exceeds the rest mass energy of muons, the rate of neutralization takes place through a new channel, $n \rightarrow p + \mu^- + \tilde{\nu}_\mu$ [20]. The presence of muons changes the proton fraction. A third channel $n \rightarrow p + \pi^-$ takes place when the chemical potential exceeds the rest mass of π^-, 139.6 MeV. Since there is no enough

Fermi energy to suppress pions with increasing the density, this channel becomes the favored mode and pions condense into the lowest state [18,19,21]. The proton fraction is of great importance in determining the cooling rate and neutrino flux within evolution of NS. The critical value of the proton fraction for direct Urca process is x_{DU} [22–24], above which the direct Urca processes $n \to p + e^- + \tilde{\nu}_e$ and $p + e^- \to n + \nu_e$ can occur and then the NS cooling rate by neutrino emission considerably increases relative to the standard cooling scenario. The Brueckner approach [22,25,26] is one of the theoretical methods used to study the proton fraction NS.

A realistic equation of state (EOS) of nuclear matter (NM) is a key input to study the nuclear structure and reactions, and some astrophysical phenomena such as the formation, composition, and merging of NS [27–31]. A series of studies have been implemented over the last few decades to understand the density and temperature dependencies of the nuclear EOS over a wide range of density and temperature [27,32–34]. Many microscopic and phenomenological nuclear approaches and various potentials have been implemented to describe the nuclear EOS, such as different forms of the M3Y nucleon-nucleon (*NN*) interaction, Gogny interaction, chiral effective-field theory, compressible liquid drop model, and quantum Monte Carlo methods [5,6,17,27,28,32,33,35–43]. For example, EOS of the NS crust determined by the compressible liquid drop model (CLDM) [44,45] in terms of the Skyrme-SLy4 interaction [46], in connection with the different regions of the NS crust. A few methods have been concerned with the dynamical evolution of hot NM and finite nuclei [16,47–49] since the pioneering work of Brack and Quentin [50] on thermal Hartree-Fock (HF) calculations. Nonrelativistic [51,52] or relativistic [53,54] types of the EOS are adopted according to investigated system, and their ability to perform ab initio calculations for the intended study. Different EOSs of the uniform NS core are obtained for the $npe\mu$ composition in the β equilibrium for cold and hot cases and extended to high densities, using different mean-field potentials. The density dependent M3Y-types of the *NN* interaction come among the trustable semirealistic interactions being used in the nuclear structure [55–57] and reaction [58–61] studies, decay modes [62–64], as well as in cold and hot NM [29,39,56,65] and astrophysical [49,66,67] investigations. In the present work, the particle fractions and the core-crust transition properties of NS and their temperature dependence will be explicitly investigated based on density dependent CDM3Y-Paris *NN* interaction. Although we could reach a fair description of the quantities under study, it remains desirable to achieve more accurate evaluation for the isovector density dependence through the investigated NS properties. In the next section, we outline the adopted theoretical framework of nuclear and thermodynamic properties of hot β stable NS matter. The numerical results are presented and discussed in Sec. III. Finally, we summarize the obtained conclusions in Sec. IV.

II. THEORETICAL FORMALISM

Considering the EOS of the uniform $npe\mu$ (npe) compositions of NS in the β equilibrium at zero and finite temperature,

the total-energy density E is given as the sum of the energy density of baryons including protons and neutrons ($E_b = E_p + E_n$) and the energy density of leptons including electrons and muons ($E_l = E_e + E_\mu$) [20,68], in addition to their rest masses. Electrons and muons can be treated as relativistic free Fermi gases, in which Coulomb contributions of energy density are negligible compared with kinetic energies [44,69]. For the density-dependent CDM3Yn [70–72] form of the M3Y [73] *NN* interaction and assuming spin saturated NM, the energy density of baryons at a given baryon density (ρ_b), isospin-asymmetry (I), and temperature (T) can be determined within the Hartree-Fock approach [29,74] as

$$E_b(T, \rho_b, I) = E_A(T, \rho_b, I) = \frac{E}{A}(T, \rho_b, I)$$
$$= E_{\text{kin}}(T, \rho_b, I) + E_{\text{pot}}(T, \rho_b, I). \quad (1)$$

The kinetic energy is given in terms of the momentum distributions of the proton (neutron) density $\rho_{p(n)}(\boldsymbol{k}, T)$ as

$$E_{\text{kin}}(T, \rho_b, I) = \frac{2}{(2\pi)^3 \rho_b} \sum_{\tau=n,p} \frac{\hbar^2}{2m_\tau} \int \rho_\tau(\boldsymbol{k}, T) k^2 d\boldsymbol{k}. \quad (2)$$

The potential-energy term is obtained as the sum of the direct and exchange contributions of both its isoscalar and isovector parts [56,70],

$$E_{\text{pot}}(T, \rho_b, I) = \varepsilon_{IS}^D(\rho_b, I) + \varepsilon_{IS}^{Ex}(T, \rho_b, I)$$
$$+ \varepsilon_{IV}^D(\rho_b, I) + \varepsilon_{IV}^{Ex}(T, \rho_b, I). \quad (3)$$

The direct (*D*) and exchange (*Ex*) parts of the CDM3Yn density dependent form of the *NN* interaction read $v_{00(01)}^{D(Ex)}(\rho_b, r) = F_{0(1)}(\rho_b) v_{00(01)}^{D(Ex)}(r)$, with density dependence of the form $F_{0(1)}(\rho_b) = C_{0(1)}(1 + \alpha_{0(1)} e^{-\beta_{0(1)}\rho_b} - \gamma_{0(1)}\rho_b)$ [39,56,70]. Here, $v_{00(01)}^{D(Ex)}(r)$ denote the radial strengths of the central direct (exchange) parts of the isoscalar (00) and isovector (01) components of M3Y *NN* interaction [65,75]. The CDM3Y density dependence of the isoscalar (IS) component of the M3Y Paris and Reid *NN* interactions has been well tested in the nuclear matter studies [39,43,65,76] and in the analysis of the elastic α-nucleus and nucleus-nucleus scattering, and in other different nuclear reactions and decays [70,72,77]. Simple formulas have been derived to parametrize the isoscalar density dependence $F_0(\rho)$ of both the M3Y-Paris and M3Y-Reid interactions in terms of the saturation properties of symmetric nuclear matter (SNM) [39]. These derived formulas can give nuclear EOS characterized by any suggested value of the saturation incompressibility coefficient (K_0) in the range from $K_0 = 150$ MeV to $K_0 = 300$ MeV [39]. On the other hand, the isovector (IV) density dependence $F_1(\rho)$ can be probed in the charge-exchange-reaction studies [78], and in some of the NS properties, as will be seen in the present study. The same functional form of the IS density dependence has been used for the IV part (DIV), with a scaling factor that is determined by fitting through experimental data of (p, n) cross section [78], or via constrains of NM observables [39]. More accurate method has been developed [79] to parametrize the IV density dependence form of the CDM3Y6 interaction using the Brueckner-Hartree-Fock (BHF) description of the

nucleon optical potential given by Jeukenne, Lejeune, and Mahaux (JLM) [80] in NM. Considering a direct relation between the single-particle (SP) potential in NM and the nuclear symmetry energy [81,82], the parameters of the IV density dependence of the CDM3Y3 and CDM3Y6 interactions have been determined independently of the corresponding IS parameters (IIV) [56]. This was done by matching the HF calculations of the IV part of the nucleon optical-potential (OP) in NM, which is performed by including a rearrangement term (RT) of the SP potential at the Fermi momentum for different NM density, with the similar BHF results obtained by JLM [80,83]. A consistent method was suggested to consider effectively the density, isospin-asymmetry, and the momentum dependence of the RT of the SP potential in the adopted HF scheme. The CDM3Yn forms of the *NN* interaction with DIV density dependence of its isovector contribution have been used to study the isobaric-analog excitation and symmetry energy [79], fusion reactions [84], neutron transition strengths of excited states in neutron-rich light isotopes from inelastic proton scattering [85], static and thermal properties of NM [86], monopole strength of the Hoyle state in inelastic α scattering [87], in addition to the asymmetric NM and its saturation properties. On the other hand, the RT was found to affect significantly the nucleus-nucleus optical potential at small internuclear distances [58], the astrophysical *S* factor of ^{12}C + ^{12}C fusion [88], and the optical model description of elastic nucleon [89] and heavy-ion scattering at low energies [90]. In the present work, we will investigate the two DIV [$F_1(\rho) = 1.1F_0(\rho)$] and IIV ($\alpha_1 \neq \alpha_0$, $\beta_1 \neq \beta_0$, $\gamma_1 \neq \gamma_0$, and $C_1 \neq C_0$) density dependence parametrizations of the M3Y-Paris *NN* interaction, for the considered EOSs. This is to investigate the consistent rearrangement effect of the nuclear mean-field potential on the NS properties.

The direct parts of the isoscalar and isovector potential-energy density respectively read

$$\varepsilon_{IS}^D(\rho_b) = \frac{\rho_b}{2}F_0(\rho_b)J_{00}^D, \tag{4a}$$

and

$$\varepsilon_{IV}^D(\rho_b, I) = \frac{\rho_b}{2}F_1(\rho_b)I^2 J_{01}^D, \tag{4b}$$

where $J_{00(01)}^D = \int v_{00(01)}^D(r)dr$, the direct parts of *NN* interaction are given as $v_{00}^D(r) = 11061.625e^{(-4r)}/(4r) - 2537.5e^{(-2.5r)}/(2.5r)$ and $v_{01}^D(r) = 313.625e^{(-4r)}/(4r) + 223.5e^{(-2.5r)}/(2.5r)$. The factor $1/2$ in Eqs. (4a) and (4b) avoids the double counting of nucleons when integrating over the total volume. The exchange (*Ex*) parts of the isoscalar and isovector potential-energy density can be respectively obtained as

$$\varepsilon_{IS}^{Ex}(T, \rho_b, I) = \frac{F_0(\rho_b)}{8\rho_b\pi^5}\int \rho(\boldsymbol{k}, T)H_{IS}(\rho, \boldsymbol{k}, I, T)d\boldsymbol{k}, \tag{5a}$$

and

$$\varepsilon_{IV}^{Ex}(T, \rho_b, I) = \frac{F_1(\rho_b)}{8\rho_b\pi^5}\int \Delta\rho(\boldsymbol{k}, T)H_{IV}(\rho, \boldsymbol{k}, I, T)d\boldsymbol{k}. \tag{5b}$$

Here, we have $\rho(\boldsymbol{k}, T) = \rho_n(\boldsymbol{k}, T) + \rho_p(\boldsymbol{k}, T)$, $\Delta\rho(\boldsymbol{k}, T) = \rho_n(\boldsymbol{k}, T) - \rho_p(\boldsymbol{k}, T)$,

$$H_{IS}(\rho_b, \boldsymbol{k}, I, T) = \int \rho(\boldsymbol{k}', T)d\boldsymbol{k}'$$
$$\times \int_0^\infty j_0(kr)j_0(k'r)v_{00}^{Ex}(r)r^2dr,$$

and

$$H_{IV}(\rho_b, \boldsymbol{k}, I, T) = \int \Delta\rho(\boldsymbol{k}', T)d\boldsymbol{k}'$$
$$\times \int_0^\infty j_0(kr)j_0(k'r)v_{01}^{Ex}(r)r^2dr.$$

The isoscalar (IS) and isovector (IV) exchange contributions of the M3Y-Paris *NN* potential respectively read $v_{00}^{Ex}(r) = -1524.25e^{(-4r)}/(4r) - 518.75e^{(-2.5r)}/(2.5r) - 7.8474e^{(-0.7072r)}/(0.7072r)$ and $v_{01}^{Ex}(r) = -4118.0e^{(-4r)}/(4r) + 1054.75e^{(-2.5r)}/(2.5r) + 2.6157e^{(-0.7072r)}/(0.7072r)$. j_0 denotes the first-order spherical Bessel function.

For hot spin-saturated nuclear matter (NM) at $T > 0$ MeV, the proton (neutron) momentum distribution can be described by the Fermi-Dirac distribution function [29,74,91],

$$\rho_{\tau=p,n}(\rho_b, \boldsymbol{k}, I, T) = \frac{1}{1 + \exp\left(\frac{\varepsilon_\tau(\rho_b, \boldsymbol{k}, I, T) - \mu_\tau}{T}\right)}. \tag{6}$$

In this equation μ_τ defines the nucleon chemical potential, while ε_τ represents the single-particle energy [29,74],

$$\varepsilon_\tau(\rho_b, \boldsymbol{k}, I, T) = \frac{\hbar^2 k^2}{2m_\tau} + U_\tau(\rho_b, \boldsymbol{k}, I, T). \tag{7}$$

The single-particle potential (U_τ) includes the isoscalar and isovector parts of both Hartree-Fock (HF) and rearrangement (RT) contributions,

$$U_\tau(\rho_b, \boldsymbol{k}, I, T) = U_{IS}^{HF}(\rho_b, \boldsymbol{k}, I, T) \pm U_{IV}^{HF}(\rho_b, \boldsymbol{k}, I, T)$$
$$+ U_{IS}^{RT}(\rho_b, I, T) + U_{IV}^{RT}(\rho_b, I, T), \tag{8}$$

where

$$U_{IS(IV)}^{HF}(\rho_b, \boldsymbol{k}, I, T) = U_{IS(IV)}^D(\rho_b, I) + U_{IS(IV)}^{Ex}(\rho_b, \boldsymbol{k}, I, T). \tag{9}$$

The positive (negative) sign in Eq. (8) applies to the neutron (proton). The nucleon chemical potential μ_τ [Eq. (6)] can be iteratively determined in connection with the single-particle potential U_τ [Eqs. (7) and (8)], under the normalization of nucleon momentum distribution to the corresponding nucleon density,

$$\frac{g}{(2\pi)^3}\int d\boldsymbol{k}\rho_{p(n)}(\rho_b, \boldsymbol{k}, I, T) = \rho_{p(n)} = (1 \pm I)\rho_b/2. \tag{10}$$

Here, the positive (negative) sign refers to the neutron (proton) density and the spin degeneracy factor is $g = 2$. For cold NM ($T = 0$ MeV), the momentum distribution of the proton (neutron) number density distribution becomes $\rho_\tau = 1$ for the momenta $k < k_{F\tau}$ and vanishes for the momenta larger than the Fermi momentum $k_{F\tau} = (3\pi^2\rho_\tau)^{1/3}$. For the CDM3Yn *NN* interaction, the temperature independent isoscalar and

isovector direct parts of the single-particle potential can be respectively written as

$$U_{IS}^D(\rho_b) = \rho F_0(\rho_b) J_{00}^D, \quad (11a)$$

and

$$U_{IV}^D(\rho_b, I) = \rho F_1(\rho_b) I J_{01}^D. \quad (11b)$$

The associated HF exchange terms read

$$U_{IS(IV)}^{Ex}(\rho_b, \boldsymbol{k}, I, T) = \frac{F_{0(1)}(\rho_b)}{\pi^2} H_{IS(IV)}(\rho_b, \boldsymbol{k}, I, T). \quad (12)$$

The isoscalar and isovector rearrangement terms in Eq. (8) can be respectively related to the corresponding direct and exchange terms as

$$U_{IS}^{(RT)}(\rho_b, I, T)$$
$$= \frac{\partial F_0(\rho_b)}{\partial \rho_b} \left[\frac{\rho_b^2}{2} J_{00}^D + \frac{1}{8\pi^5} \int \rho(\boldsymbol{k}, T) H_{IS} d\boldsymbol{k} \right], \quad (13a)$$

and

$$U_{IV}^{(RT)}(\rho_b, I, T)$$
$$= \frac{\partial F_1(\rho_b)}{\partial \rho_b} \left[\frac{I^2 \rho_b^2}{2} J_{01}^D + \frac{1}{8\pi^5} \int \Delta\rho(\boldsymbol{k}, T) H_{IV} d\boldsymbol{k} \right]. \quad (13b)$$

The evolution of the entropy of hot asymmetric nuclear matter (ANM) controls its thermodynamic equilibrium. One can calculate the entropy per nucleon for hot ANM at finite temperature T and nucleon density ρ_b as [29,74,92],

$$S_A(T, \rho_b, I)$$
$$= \frac{g}{8\pi^3 \rho_b} \sum_{\tau=p,n} \int \{\rho_\tau(\rho_b, \boldsymbol{k}, I, T) \ln [\rho_\tau(\rho_b, \boldsymbol{k}, I, T)]$$
$$+ [1 - \rho_\tau(\rho_b, \boldsymbol{k}, I, T)] \ln [1 - \rho_\tau(\rho_b, \boldsymbol{k}, I, T)]\} d\boldsymbol{k}. \quad (14)$$

In terms of the internal energy per nucleon (E_A) and the entropy per nucleon (S_A), the Helmholtz free energy per nucleon, $F_A(T, \rho_b, I)$, of the hot ANM reads

$$F_A(T, \rho_b, I) = \frac{F(T, \rho_b, I)}{A} = E_A(T, \rho_b, I) - TS_A(T, \rho_b, I). \quad (15)$$

The number densities of electrons and muons are determined from the charge neutrality condition $\rho_p = \rho_e + \rho_\mu$ and upon dividing by the number density ρ we get $x_p = x_e + x_\mu$, where x_p, x_e, and x_μ respectively represent the proton, electron and muon fractions. For cold NM, muons start to appear at $\rho \geqslant \rho_0$ with a little contribution to the chemical equilibrium because they require high electronic chemical potential greater than or equal to the rest mass energy of muons, $\mu_e \geqslant m_\mu c^2 = 105.66$ MeV [20]. In β-stable ($npe\mu$) matter of a NS, the chemical equilibrium of the direct URCA reactions ($n \to p + e^- + \tilde{\nu}_e$ and $p + e^- \to n + \nu_e$) thermodynamically yields [93]

$$\mu_e = \mu_\mu = \mu_n - \mu_p = 2\frac{\partial F_A(T, \rho_b, I)}{\partial I} = -\frac{\partial F_A(T, \rho_b, x_p)}{\partial x_p}. \quad (16)$$

The chemical potential of the relativistic electrons at $T = 0$ MeV can be determined in terms of the total density of baryons and leptons (ρ) as [43,49]

$$\mu_e = \sqrt{k_{Fe}^2 c^2 + m_e^2 c^4} \approx k_{Fe} c = \hbar c (3\pi^2 \rho x_e). \quad (17)$$

Upon Eqs. (16) and (17) and applying the charge neutrality condition ($x_p = x_e$ for $\rho < \rho_0$ and $x_p = x_e + x_\mu$ for $\rho \geqslant \rho_0$), the p, e, and μ fractions can be obtained at $T = 0$ MeV by solving the equation [43,49],

$$3\pi^2 (\hbar c)^3 \rho x_p - \mu_e^3 - \left[\mu_e^2 - (m_\mu c^2)^2\right]^{3/2} \theta(\mu_e - m_\mu c^2) = 0. \quad (18)$$

The Heaviside step function $\theta(\mu_e - m_\mu c^2)$ is equal to zero for $\mu_e < m_\mu c^2$ and it becomes 1 otherwise. At finite temperature $T > 0$ MeV, the e and μ number densities can be determined as [14,94]

$$\rho_{e(\mu)} = \rho x_{e(\mu)} = \frac{1}{\pi^2} \int_0^\infty \frac{dk k^2}{1 + \exp\left(\frac{\sqrt{\hbar^2 c^2 k^2 + m_{e(\mu)}^2 c^4} - \mu_{e(\mu)}}{T}\right)}, \quad (19)$$

which is similar to Eq. (10). Equations (16) and (19) are then solved together along with $x_p = x_e + x_\mu$ in a self-consistent manner to obtain the p, e, and μ fractions at finite temperature $T > 0$ MeV.

In terms of the e and μ fractions, the Direct Urca (DU) threshold value for the proton fraction, above which the DU becomes possible, can be given as [22]

$$x_{DU} = \frac{1}{1 + \left(1 + r_e^{1/3}\right)^3}, \quad (20)$$

where $r_e = 1/[1 + (x_\mu/x_e)]$ is the leptonic electron fraction. This yields $x_{DU} = 1/9$ for $\rho < \rho_0$ and $x_{DU} > 1/9$ for $\rho \geqslant \rho_0$ [23,95,96]. This is according to the momentum conservation, where with increasing density the Fermi momenta of proton and electrons increase faster than that of neutrons. The total pressure of the $npe\mu$ matter is the sum of the pressures of baryons [39,43], electrons, and muons [20,43,68] and can be then obtained at $T = 0$ MeV as

$$P(\rho, x_p, x_e, x_\mu) = \rho^2 \frac{\partial E_A(\rho, x_p)}{\partial \rho} + \frac{\hbar c}{12\pi^2}\left(3\pi^2 \rho x_e\right)^{4/3} + P_\mu(\rho, x_\mu). \quad (21)$$

The total pressure of the $npe\mu$ matter at finite temperature $T > 0$ MeV is obtained as the sum of the baryons [29], and leptons [94] pressure contributions as

$$P(T, \rho, x_p, x_e, x_\mu) = \rho^2 \frac{\partial F_A(T, \rho, x_p)}{\partial \rho} + \sum_{\ell=e,\mu} P_\ell(T, \rho, x_\ell),$$

$$P_\ell(T, \rho, x_\ell) = \frac{(\hbar c)^2}{3\pi^2} \int_0^\infty \frac{dk k^4 (\hbar^2 c^2 k^2 + m_\ell^2 c^4)^{-1/2}}{1 + \exp\left(\frac{\sqrt{\hbar^2 c^2 k^2 + m_\ell^2 c^4} - \mu_\ell}{T}\right)}. \quad (22)$$

The baryonic pressure is usually very large compared with that of leptons. The thermal pressure P_{th} can be defined as the difference between the pressure at a certain temperature T and

the pressure at $T = 0$. The intrinsic stability condition of a single phase for locally neutral matter under β equilibrium can be thermodynamically determined by the positivity of the matter compressibility (K_μ), at constant chemical potential [43,97],

$$K_\mu = \frac{K(T, \rho, I)}{9} - \frac{\left(\rho \frac{\partial^2 E_A(T,\rho,I)}{\partial \rho \partial I} \right)^2}{\frac{\partial^2 E_A(T,\rho,I)}{\partial I^2}} > 0, \qquad (23)$$

where

$$K(T, \rho, I) = 9 \left(2\rho \frac{\partial E_A(T, \rho, I)}{\partial \rho} + \rho^2 \frac{\partial^2 E_A(T, \rho, I)}{\partial \rho^2} \right)$$

defines the incompressibility coefficient of ANM [39,43]. The last term in Eq. (23) arises from the leptonic pressure. The transition density, proton fraction, and pressure at the boundary between the liquid core and solid crust of NS can be then obtained by solving Eq. (23).

III. RESULTS AND DISCUSSION

In the following, we investigate the temperature dependence of the considered properties and quantities within the core of a neutron star and at the borderline between the liquid core and its solid crust. Two equations of state of hot asymmetric nuclear matter (ANM) based on M3Y-Paris NN effective interaction will be considered in their CDM3Y density dependent form, namely CDM3Y3-218 and CDM3Y6-252. These two parametrizations of the density dependent forms of the M3Y-Paris NN interaction are characterized with SNM saturation incompressibility value of $K_0 = 218$ MeV and 252 MeV, respectively. Two parametrizations of the density dependence of the isovector part of the NN force will be considered, the one derived in terms of the density dependence of the isoscalar part (DIV) and the one independently derived (IIV), as described in Sec. II.

Displayed in Fig. 1 is the density dependence of the proton fraction (x_p) in cold ($T = 0$ MeV) β-stable npe [Fig. 1(a)] and $npe\mu$ [Fig. 1(b)] NS matter. Equations (17) and (18) have been used to calculate the proton fraction, respectively. The proton fraction significantly affects the neutrino emission, and consequently the thermal evolution of neutron stars. For the npe matter, the calculations based on the IIV density dependence of the isovector NN interaction show that the proton fraction increases almost linearly with increasing the ANM baryon density. The CDM3Y3-218 with IIV density dependence yields a proton fraction of $x_p = 0.286$ at density of 10 times the saturation nuclear density ($10\rho_0$). The stiffer EOS based on the CDM3Y6-252 yields less proton fraction at the same density, x_p ($\rho = 1.7$ fm^{-3}) = 0.236 and $x_n = 0.764$. Such large density values are expected at the center of NS. The difference between the indicated values of x_p increases with increasing the ANM density, reaching 0.05 at the density of $10\rho_0$. This means that the proton fraction decreases upon increasing the stiffness of the EOS and the ANM matter of NS becomes less neutron rich at its core center. The stiffness of the EOS does not affect the proton fraction indicated at the low density below $2\rho_0$. According to the CDM3Y3-218 (IIV) and CDM3Y6-252 (IIV) equations of state and in view
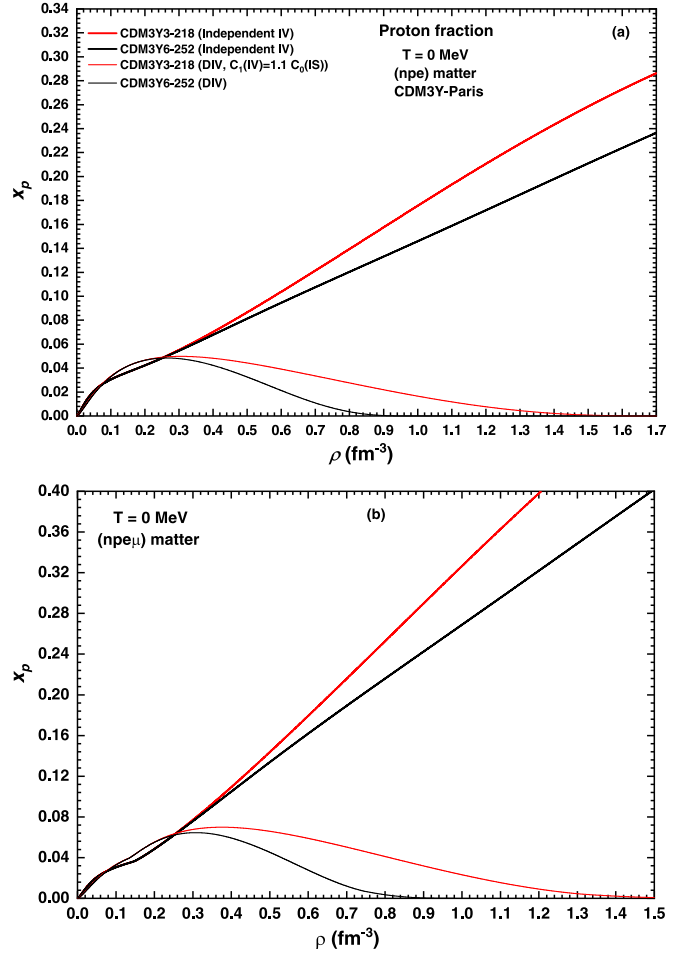

FIG. 1. Density dependence of the proton fraction (x_p) in β stable cold (a) npe and (b) $npe\mu$ matters, based on the M3Y-Paris NN interaction using two EOSs CDM3Y3 ($K_0 = 218$ MeV) and CDM3Y6 ($K_0 = 252$ MeV), with the density dependence of the isovector part of the NN force that derived in terms of the corresponding isoscalar density dependence (DIV) [70] and that derived independently (IIV) [56].

of the indicated threshold value of $x_p = 1/9$ that is imposed on proton fraction for a direct URCA process [23,96], the DU process would be possible at the densities larger than $3.7\rho_0$ and $4.3\rho_0$, respectively. Thus, the softer EOS indicates a wider range for DU process inside NS. The proton fraction based on the DIV density dependence of the isovector NN interaction is substantially different from that calculated based on the IIV parametrization of the isovector density dependence. For the cold npe matter in Fig. 1(a), the β-stable proton fraction increases upon increasing the low density reaching its maximum value of about ($x_p \approx 0.05$) within a density of about $1.5\rho_0$. Thereafter, it starts to decrease with increasing the larger density. The softer EOS still indicating larger proton fraction for the same density. According to the maximum values obtained for the proton fraction in the β-stable cold npe matter based on the CDM3Y (DIV) calculations, a prospective direct URCA process in NS would not be allowed. If this is the case, it gives rise to the slow cooling process of NS through a modified URCA process [8] and neutrino-pair emission [98],
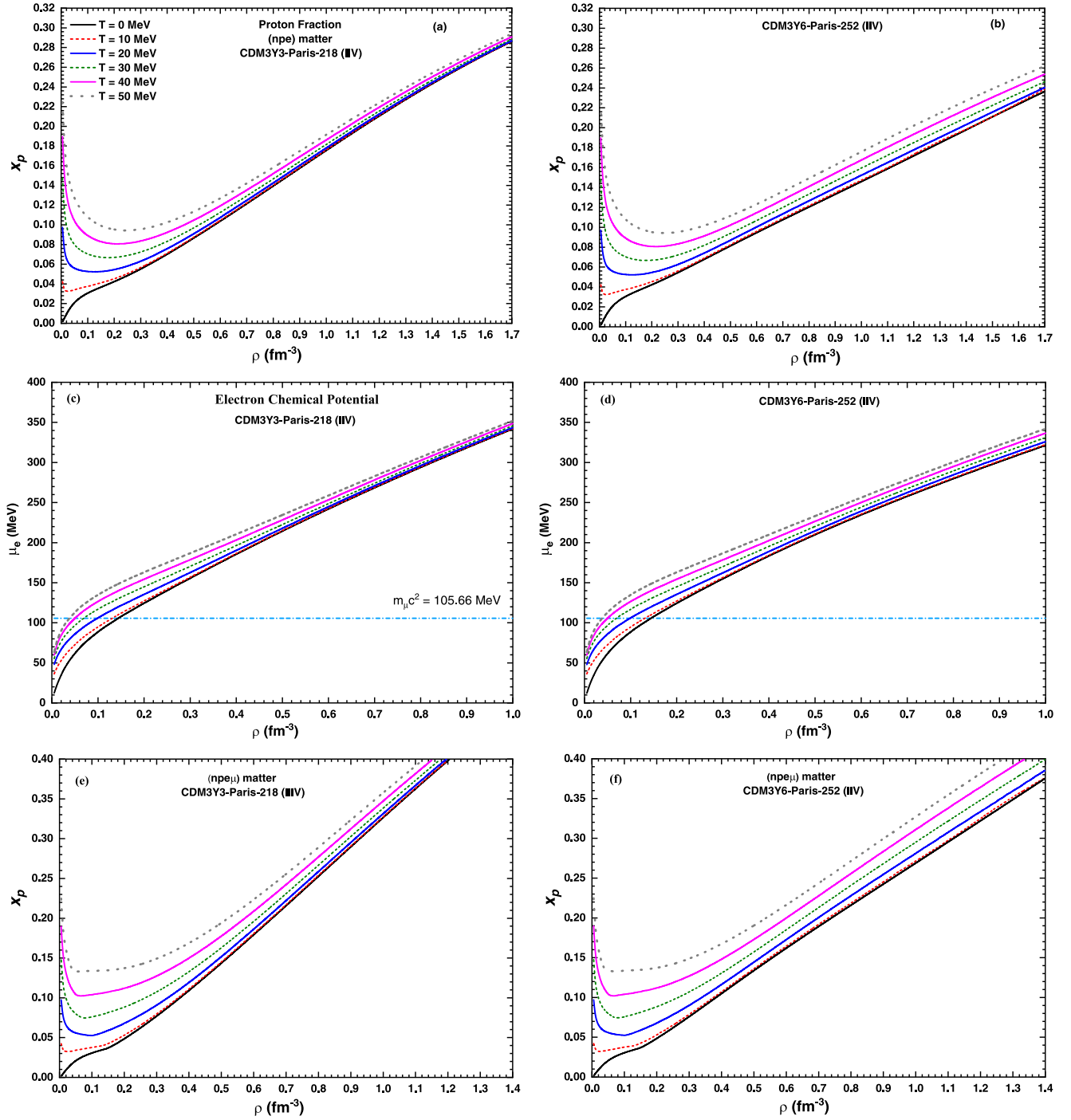
FIG. 2. Density dependence of the proton fraction in β stable npe matter based on the density-dependent (a) CDM3Y3-Paris-218 (IIV) and (b) CDM3Y6-Paris-252 (IV) NN interaction at temperatures $T = 0, 10, 20, 30, 40$, and 50 MeV represented. Panels (c) and (d) show the corresponding electron chemical potentials for the two EOSs, respectively. Panels (e) and (f) show the same as panels (a) and (b), respectively, but for $npe\mu$ matter.

as alternative cooling processes. Generally, taking account of the consistent rearrangement effect of the NN potential using the modified CDM3Y (IIV) forms yields more realistic proton fraction of NS matter.

Regarding cold β-stable $npe\mu$ matter, Fig. 1(b) shows that calculations based on the same EOSs that used in Fig. 1(a) yield a typical behavior of proton fraction as a function of

density, but with slightly larger values of x_p than it if muons are absent [Fig. 1(a)]. For cold NM, muons appear at $\rho \geqslant \rho_0$ if $\mu_e \geqslant 105.66$ MeV. The presence of muons increases the indicated values of proton fraction at the density of $10\rho_0$ to x_p ($\rho = 1.7$ fm^{-3}) > 0.5 and =0.456, based on the CDM3Y3-218 (IIV) and CDM3Y6-252 (IIV) EOSs, respectively. The difference between the indicated values of $x_p(npe\mu)$ and

$x_p(npe)$ is then about 0.22 at the density of $10\rho_0$. Based on the obtained electron and muon fractions and using Eq. (20), the DU threshold is determined to be $x_{DU}(\rho = 2.84\rho_0) = 0.137$ and $x_{DU}(\rho = 3.02\rho_0) = 0.1374$ for the CDM3Y3-218 (IIV) and CDM3Y6-252 (IIV) EOSs, respectively. Thus, the appearance of muons makes the NS tends to be less neutron-rich at its core center and decreases the density at which the DU process can takes place inside NS. The presence of muons also slightly increases the indicated maximum value of $x_p(npe\mu)$ relative to $x_p(npe)$ and its corresponding density. The density dependence of the isovector part of the CDM3Y forms of the M3Y NN force which is parametrized independently of that of the isoscalar term is the one successfully indicating the large possibility of direct URCA cooling process in NS.

It is more appropriate now to consider hot nuclear matter. The proton fraction in hot ($T = 10 - 50$ MeV) npe matter of NS is compared within a wide density range up to $10\rho_0$ with that of cold matter in Figs. 2(a) and 2(b), based on the CDM3Y3-218 (IIV) and CDM3Y6-252 (IIV) EOSs, respectively. Figures 2(a) and 2(b) show that the proton fraction as extracted based on the two considered EOSs exhibits almost the same density and temperature behaviors for npe matter. Generally, the proton fraction increases with increasing T. The increasing rate of x_p with T increases at the higher-temperature region, but it decreases with increasing the density. Below $T = 10$ MeV, Figs. 2(a) and 2(b) show that the proton fraction increases with increasing the density over the whole density range. Starting from $T = 10$ MeV, a different behavior is obtained within the low-density region around the cold saturation density where x_p decreases with density reaching a minimum value around ρ_0, then it starts to increase steadily with density. Upon increasing the temperature of the ANM, minimum value indicated for proton fraction increases and shifts to a larger corresponding density. The obtained minima based on the two mentioned EOSs in Figs. 2(a) and 2(b) are ranging from $x_p = 0.032$ (at $0.18\rho_0$) at $T = 10$ MeV to 0.094 ($1.47\rho_0$) at 50 MeV, with almost no change due to the change of the stiffness of the EOS. According to the threshold of DU process for npe, the calculations based on the two EOSs show that the density at which DU would be possible decreases from $\rho = (4.0 \pm 0.3)\rho_0$ at temperatures of $T = 0$ MeV to $(2.9 \pm 0.1)\rho_0$ at $T = 50$ MeV. Thus, increasing temperature indicates a wider range for DU process inside NS, from its core center towards the inner surface.

For hot β-stable $npe\mu$ matter, Figs. 2(c) and 2(d) show the density dependence of the electron chemical potential based on EOSs used in Figs. 2(a) and 2(b). Figures 2(c) and 2(d) show that μ_e increases upon increasing the temperature of NM. In view of the β-equilibrium for hot NM hot $npe\mu$ matter, muons is then expected to appear at lower density where μ_e gets larger than the muon mass at less density than that of $T = 0$ MeV. The saturation density also decreases upon increasing the temperature and even disappears at temperatures larger than 13 MeV [74]. Figures 2(c) and 2(d) indicate that muons possibly appear at densities of $0.9\rho_0$, $0.8\rho_0$, $0.6\rho_0$, $0.5\rho_0$, $0.3\rho_0$, and $0.2\rho_0$ at temperatures of 0, 10, 20, 30, 40, and 50 MeV, respectively. Figures 2(e) and 2(f) represent the temperature dependence of the proton fraction for hot β-stable $npe\mu$ matter, based on the same EOSs used in
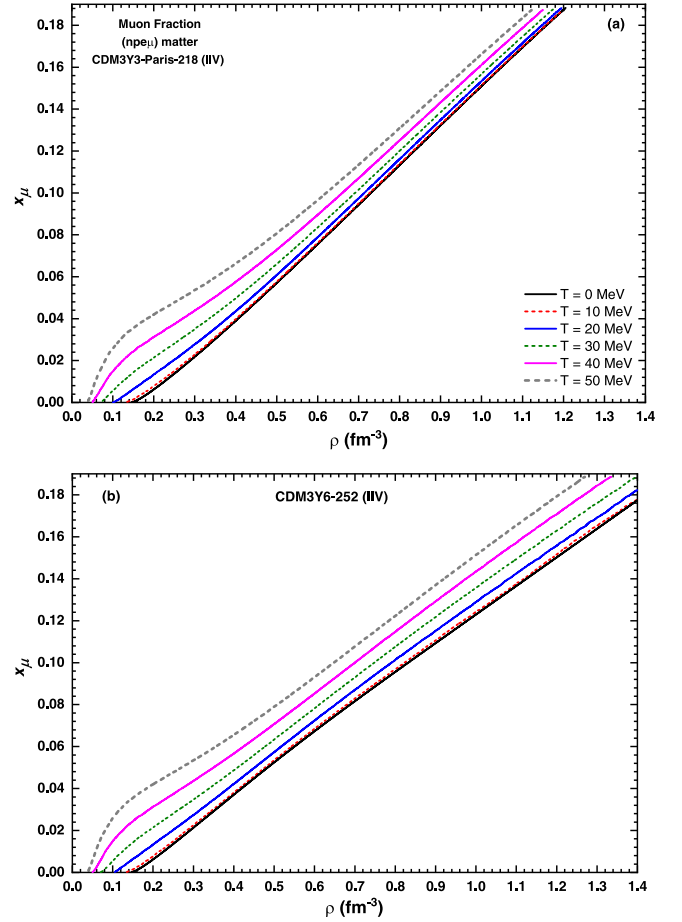

FIG. 3. Same as Figs. 2(c) and 2(d) but for the muon fraction (x_μ).

Figs. 2(a) and 2(b), respectively, and within the same density and temperature displayed in them. The corresponding muon fraction (x_μ) is displayed in Figs. 3(a) and 3(b), respectively. The appearance of muons shifts the minimum obtained values of x_p for the temperatures larger than 10 MeV to be within the same low density values at which muons start to appear, and the proton fraction starts to increase steadily with increasing density above these values. Muons also increase the values of x_p at the high density of $10\rho_0$ to about 150% relative to the muon-free matter, for all displayed temperatures. The obtained DU threshold in presence of muons slightly decreases from $x_{DU}(\rho = (2.9 \pm 0.1)\rho_0) = 0.14$ at $T = 0$ MeV to 0.12 ($0.5\rho_0$) at 50 MeV. Thus, the decrease in the threshold density value of DU due to the inclusion of muons increases with increasing the temperature. Increasing the temperature still decreasing the density at which the threshold x_{DU} value is verified, indicating a wider range for DU process inside NSs. Thus, muons start to appear within the outer core of NSs at densities lower than ρ_0 when the electron Fermi energy surpasses the rest mass energy of muons, as shown in Figs. 2(c) and 2(d). Figure 3 shows that the amount of muons at a given density of $npe\mu$ matter of NSs increases with increasing its temperature. Based on the two considered EOSs, the muon fraction at ρ_0 increases from $x_\mu \approx 0.002$ at $T = 0$ to 0.038 at 50 MeV. x_μ increases linearly upon increasing the nuclear
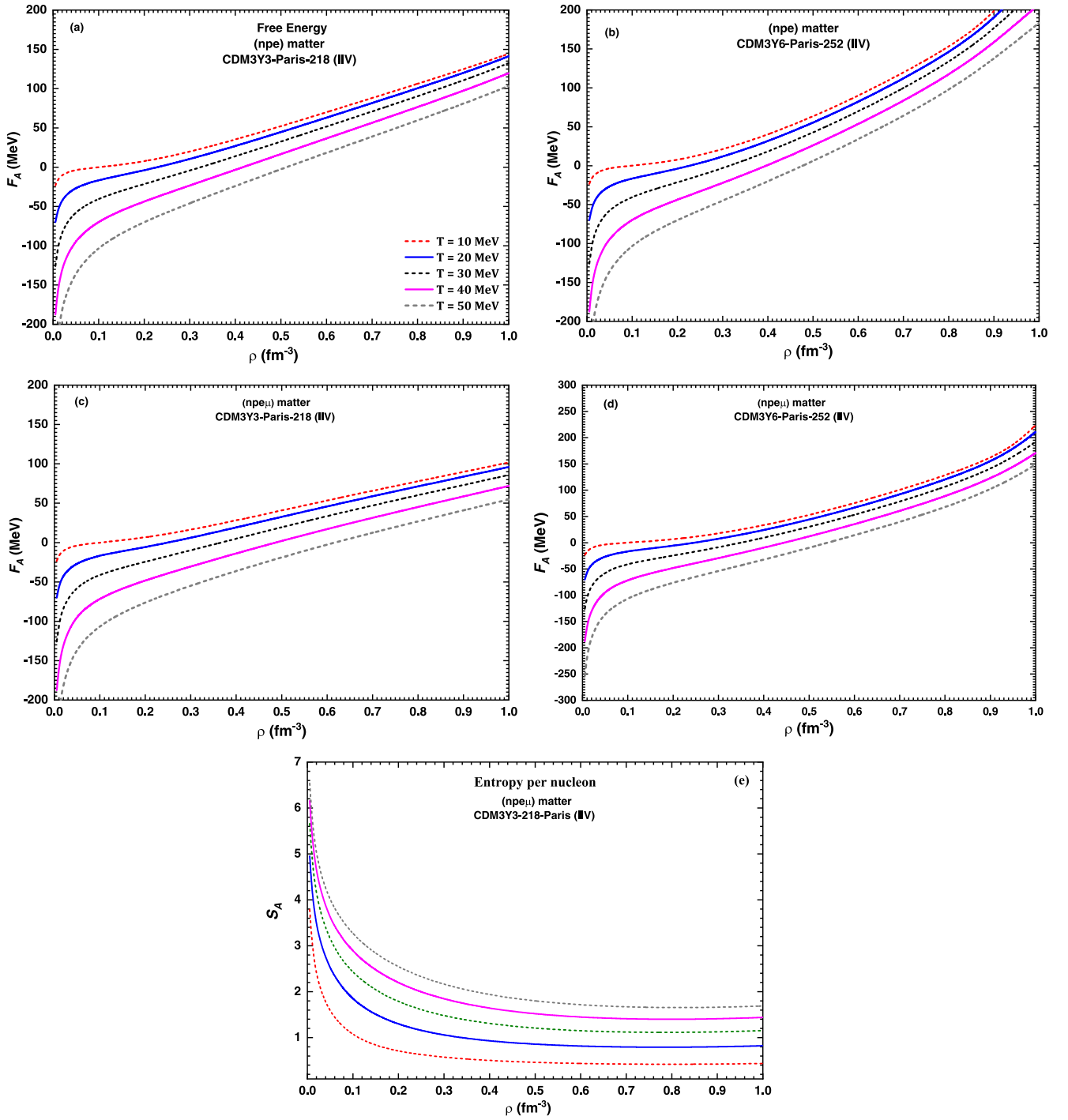
FIG. 4. (a)–(d) Same as Figs. 2(a), 2(b), 2(e), and 2(f), respectively, but for the free energy of baryons [Eq. (15)] over the density range $\rho \leqslant 1$ fm^{-3}. (e) Same as Fig. 4(c) but for the entropy per nucleon.

matter density. For the different temperatures, x_μ reaches about $0.5x_p$ within the high-density region.

Displayed in Figs. 4 and 5 are the density and temperature dependencies of the mapping of the thermodynamical Helmholtz free energy of baryons [Eq. (15)] and of the thermal pressure of NS matter, including baryons and leptons on the proton fraction graphs in the different panels of Fig. 2, over the temperature and density ranges up to 50 MeV and 1 fm^{-3}, respectively. Figures 4(a)–4(d) show that the attractive free

energy per nucleon (F_A) decreases (increases) with increasing the density (temperature) of the NS matter. This is expected where the substantial increase of the entropy S_A with T leads to a larger increase of the subtracted $T S_A$ term in Eq. (15) than the increase in leading term of binding energy E_A. Consequently, the attractive free energy decreases with T. The free energy becomes repulsive after a few multiplies of the saturation density. The density at which the free energy starts to be repulsive increases from about $0.5\rho_0$ at $T = 10$ MeV to
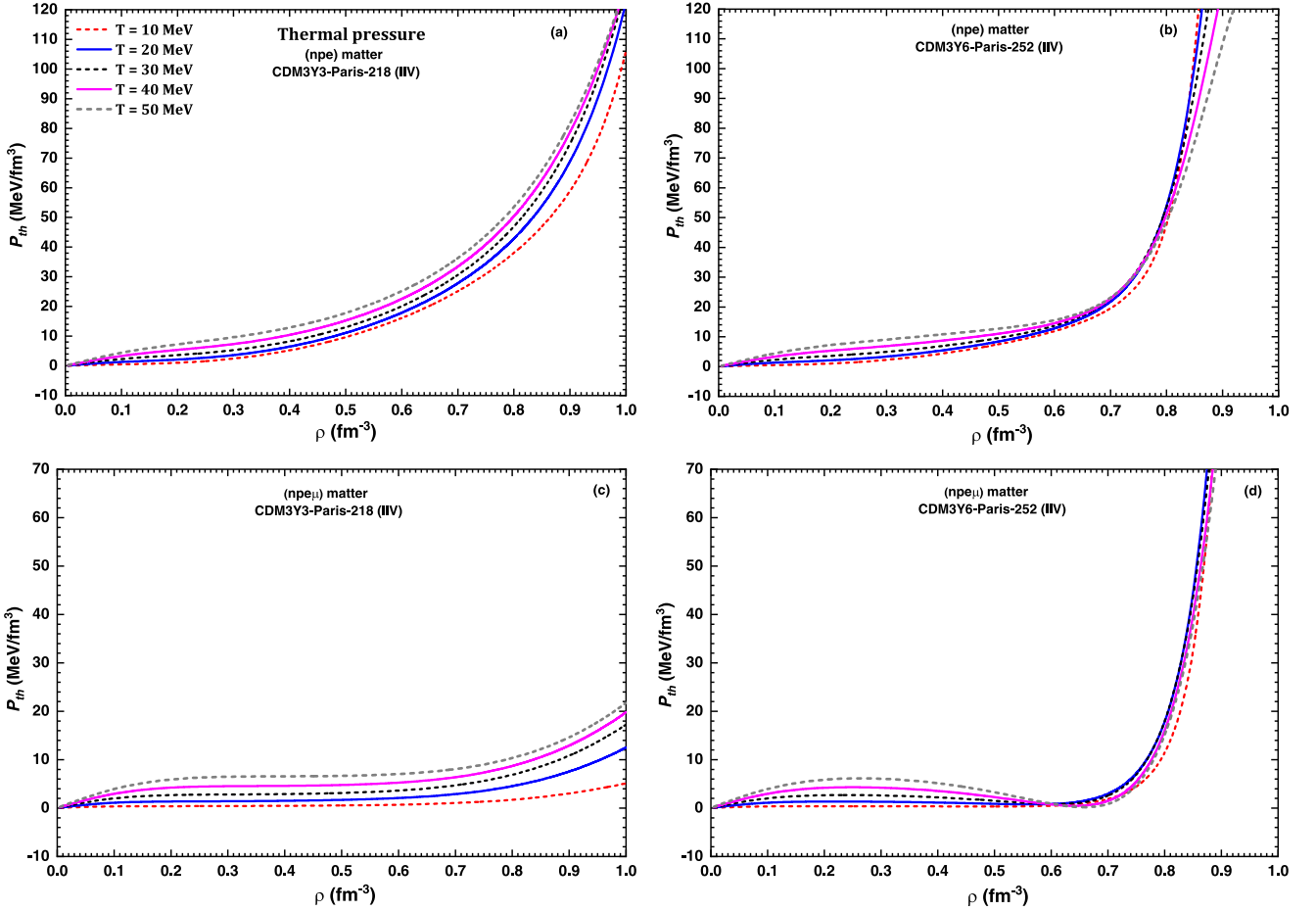
FIG. 5. Same as Fig. 2 but for the thermal pressure, $P_{th} = P(T) - P(0)$, inside NSs, over the density range $\rho \leqslant 1$ fm^{-3}.

about $3\rho_0$ at $T = 50$ MeV. The repulsive F_A at high density increases with increasing the stiffness of the NS matter, and decreases upon the inclusion of muons, as can be seen in the different panels of Fig. 4. The density and temperature dependencies of the entropy per nucleon (S_A) of the hot $npe\mu$ matter within the considered temperature range is shown in Fig. 4(e), based on the CDM3Y3-218 (IIV) EOS, as an example.

The thermal pressure, $P_{th} = P(T) - P(0)$, of the NS matter in Fig. 5 is calculated using the pressure given by Eqs. (21) and (22). The pressure of baryons is predominant compared with that of leptons because of their great masses and high fractions relative to leptons. As seen in Fig. (5), the thermal pressure increases monotonically with density and temperature. This ensures stability condition $\frac{dP}{d\rho} \geqslant 0$ of the NS matter [69,99]. Three competing effects influence the behavior of thermal pressure with density and temperature [31], namely the individual thermal pressures of neutrons and protons which increase with density, the isospin asymmetry that decreases with temperature and then decreases the total pressure, and finally increasing the thermal pressure of leptons upon increasing the lepton fraction. Figure 5 shows that the thermal pressure starts with a weak density dependence in the low-density region up to about $3\rho_0$ ($4\rho_0$) in the absence (presence) of muons, then it grows stronger at the higher densities. The density dependence of pressure is generally

stronger than its temperature dependence. Increasing the stiffness of the EOS slightly decreases P_{th} in the density range up to about $4\rho_0$, and increases it otherwise. The inclusion of muons decreases the thermal pressure to lower values as seen in Figs. 5(c) and 5(d).

Figure 6(a) presents the temperature dependence of the liquid core-solid crust transition density in NS as extracted from the calculations of the incompressibility condition [Eq. (23)] based on the M3Y Paris NN interaction within the temperature range $T = 0$–50 MeV, using the CDM3Y3-218 (DIV), CDM3Y6-252 (DIV), CDM3Y3-218 (IIV), and CDM3Y6-252 (IIV) EOSs. The corresponding transition proton fraction and pressure [Eqs. (18) and (19)] are respectively displayed in Figs. 6(b) and 6(c). As seen above, the four considered EOSs successfully describe the proton fraction for the densities up to $1.5\rho_0$. Also, no muons are appearing within the obtained transition density region. As seen in Fig. 6(a), the core-crust transition density is estimated for cold NM at $T = 0$ MeV within the range of $(0.54 \pm 0.02)\rho_0$. The transition density from the core to the crust increases upon increasing the temperature, reaching a value of about $(0.85 \pm 0.04)\rho_0$ at $T = 50$ MeV. The corresponding transition proton fraction (pressure) increases steadily with temperature from $x_{pt} = 0.03$ ($P_t = 0.36 \pm 0.12$ MeV fm^{-3}) at $T = 0$ MeV to about 0.14 (7.36 ± 0.52 MeV fm^{-3}) at $T = 50$ MeV. However, the
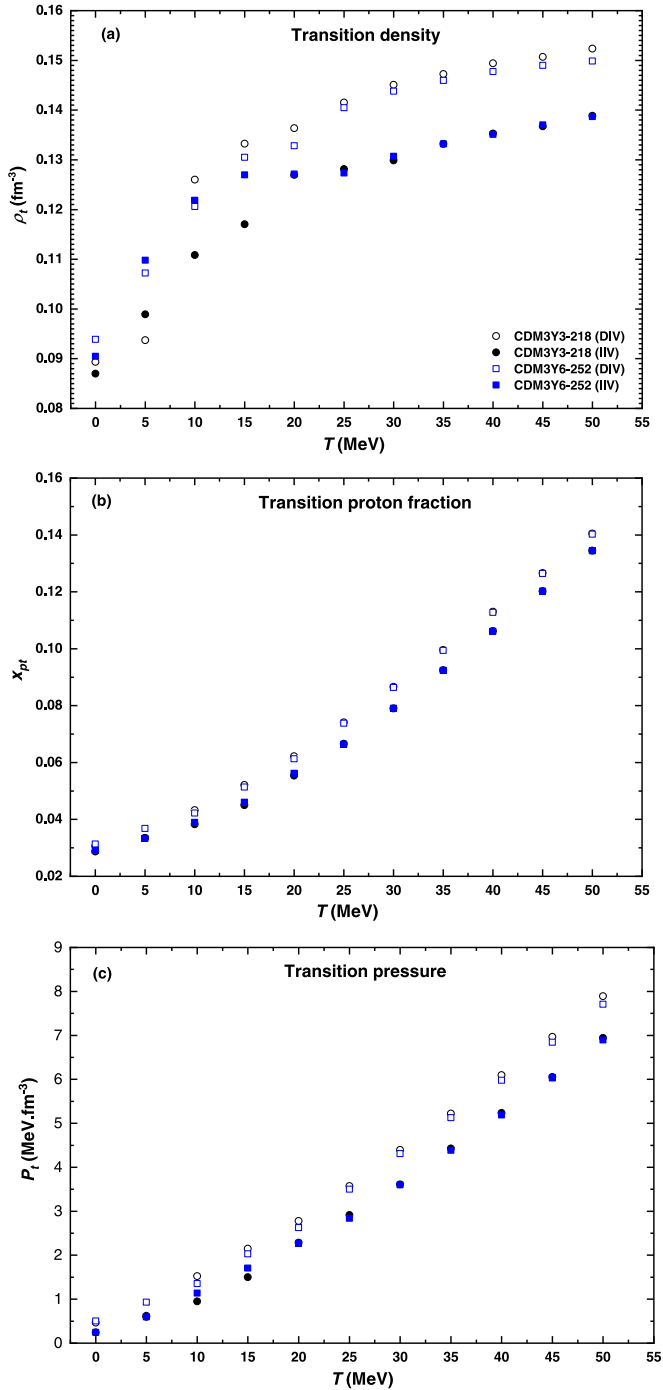
FIG. 6. Temperature dependence of the core-crust (a) transition density ρ_t (fm^{-3}) [Eq. (23)], (b) transition proton fraction x_{pt} [Eqs. (17) and (18)], and (c) transition pressure P_t (MeV fm^{-3}) [Eqs. (21) and (22)] in NSs based on the CDM3Y3-218 (DIV), CDM3Y6-252 (DIV), CDM3Y3-218 (IIV), and CDM3Y6-252 (IIV) EOSs.

constraints obtained here on the core-crust transition density and pressure at $T = 0$ MeV are consistent with those obtained in few similar studies [27,100] but they are slightly higher than those obtained in other studies [20,101]. For example, using a modified Gogny (MDI) and 51 Skyrme interactions, within both dynamical and thermodynamical

methods, slightly lower limits of $\rho_t = (0.52 \pm 0.02)\rho_0$ and $P_t = 0.13 \pm 0.12$ MeV fm^{-3} are imposed from constraints on the symmetry energy by the isospin diffusion data in HI collisions [20]. Also, the calculations performed in terms of the isospin asymmetry expansion of the EOS including the terms up to E_{sym4} within a nonlinear relativistic mean-field model based on the calibrated FSUGold and IU-FSU interactions gave lower $\rho_t = (0.38 \pm 0.08)\rho_0$ but similar $P_t = 0.39 \pm 0.15$ MeV fm^{-3} [101]. Furthermore, estimated constraints of slightly lower $\rho_t = (0.52 \pm 0.01)\rho_0$ and slightly larger $P_t = 0.53 \pm 0.23$ MeV fm^{-3} have been obtained in the framework of relativistic nuclear energy density functional, with adjusted functional to the binding energies of finite nuclei and their isovector properties [100]. Using EOSs of 220 MeV $\leqslant K_0 \leqslant$ 270 MeV in terms of CDM3Y density dependent Paris and Reid NN interactions, consistent ranges of $\rho_t = (0.55 \pm 0.02)\rho_0$, $P_t = 0.54 \pm 0.05$ MeV fm^{-3}, and $x_{pt} = 0.03$, were estimated for cold NM [43]. Moreover, using four exact expressions of the energy density based on finite-range simple effective interaction (SEI), ranges of $\rho_t = (0.47 \pm 0.02)\rho_0$, $P_t = 0.43 \pm 0.10$ MeV fm^{-3} were obtained [102]. As the core-crust transition quantities are very uncertain and highly model dependent [103], the results obtained in the present work for their temperature dependence will shed light on the structure of hot NS.

IV. SUMMARY AND CONCLUSIONS

We investigated thermodynamically the core-crust transition at the inner edge of neutron stars and its temperature dependence. We analytically expressed the intrinsic stability condition of the core-crust transition, and consequently the transition density and pressure as well as the proton fraction of the npe ($npe\mu$) matter under β equilibrium, based on exact EOS in the framework of a nonrelativistic Hartree-Fock scheme. We considered two EOSs characterized with SNM saturation incompressibility range of $K_0 = 218$ MeV and 252 MeV, based on two parametrizations of the density dependence of the isovector part of the M3Y force for each EOS. While one of the adopted IV density dependence was derived in terms of the IS density dependence (DIV), the other one was derived independently of it (IIV). The inclusion of the consistent rearrangement effect of the mean-field NN potential using the modified CDM3Y (IIV) forms of the NN interactions is found to be essential to obtain accurate proton fraction of NS matter. We found that increasing the stiffness of the EOS decreases the proton fraction of the NS matter, and makes it less neutron-rich at the core center. The softer EOS indicates a wider range for DU process inside NS from its core center. Also, increasing the temperature decreases the density corresponding to the threshold x_{DU} value, indicating a wider range for DU process inside NS. The appearance of muons decreases the isospin asymmetry of the NS matter at its core center and decreases the threshold density of DU, increasing slightly the values of proton fraction at the high density of $10\rho_0$ slightly relative to the muon-free matter. While x_μ is linearly increases with nuclear matter density, it slightly increases with temperature. Over the different temperatures up to 50 MeV, the β-stable muon fraction of $npe\mu$ matter is

inferred to have a value of about $0.5x_\mu$ at high matter density. The density dependence of the thermal pressure is generally stronger than its temperature dependence. It becomes stronger at the higher densities. Appearing of muons decreases the thermal pressure of the $npe\mu$ matter, relative to the npe matter. Based on the four considered EOSs in terms of the CDM3Y-Paris interaction, the core-crust transition density, pressure, and proton fraction are estimated for cold NM within the ranges of $(0.54 \pm 0.02)\rho_0$, 0.36 ± 0.12 MeV fm^{-3}, and 0.03, respectively. These estimated values are increased with temperature reaching $(0.85 \pm 0.04)\rho_0$, 7.36 ± 0.52 MeV fm^{-3}, and 0.14, respectively, at $T = 50$ MeV. In view of the uncertainty concerning the estimated values of the core-crust transition quantities and their model dependence, the results obtained here and its temperature dependence would help in clearing up the structure of hot NS.

[1] P. Haensel, A. Y. Potekhin, and D. G. Yakovlev, *Neutron Stars 1* (Springer-Verlag, New York, 2007).

[2] L. Rezzolla, P. Pizzochero, D. I. Jones, N. Rea, and I. Vidaña, *The Physics and Astrophysics of Neutron Stars* (Springer, Switzerland, 2018).

[3] H.-T. Janka, K. Langanke, A. Marek, G. Martínez-Pinedo, and B. Müller, Phys. Rep. **442**, 38 (2007).

[4] R. Buras, M. Rampp, H.-T. Janka, and K. Kifonidis, Phys. Rev. Lett. **90**, 241101 (2003).

[5] T. Kawamoto and Y. Kabashima, Phys. Rev. E **97**, 022315 (2018).

[6] I. Tews, Phys. Rev. C **95**, 015803 (2017).

[7] G. F. Burgio and I. Vidaña, Universe **6**, 119 (2020).

[8] J. M. Lattimer and M. Prakash, Science **304**, 536 (2004).

[9] I. Sagert and J. Schaffner-Bielich, Astron. Astrophys. **489**, 281 (2008).

[10] J. S. Read, B. D. Lackey, B. J. Owen, and J. L. Friedman, Phys. Rev. D **79**, 124032 (2009).

[11] C. A. Raithel, F. Özel, and D. Psaltis, Astrophys. J. Lett. **844**, 156 (2017).

[12] B. Friedman and V. R. Pandharipande, Nucl. Phys. A **361**, 502 (1981).

[13] T. Takatsuka, Prog. Theor. Phys. **95**, 901 (1996).

[14] L. Chen, F. Zhang, Z. Lu, and W. Li, J. Phys. G **27**, 1799 (2001).

[15] James M. Lattimer, Gen. Relativ. Gravit. **46**, 1713 (2014).

[16] H. Shen, H. Toki, K. Oyamatsu, and K. Sumiyoshi, Prog. Theor. Phys. **100**, 1013 (1998).

[17] A. Roggero, A. Mukherjee, and F. Pederiva, Phys. Rev. Lett. **112**, 221103 (2014).

[18] C. Feng-Shou, and Z. Lie-Wen, Chin. Phys. Lett. **18**, 142 (2001).

[19] H. Greiner, *Walter and Stöcker* (Springer Science & Business Media, 2013).

[20] J. Xu, L.-W. Chen, B.-A. Li, and H.-R. Ma, Astrophys. J. **697**, 1549 (2009).

[21] C. A. Raithel, F. Özel, and D. Psaltis, Astrophys. J. **875**, 12 (2019).

[22] T. Klähn, D. Blaschke, S. Typel, E. N. E. van Dalen, A. Faessler, C. Fuchs, T. Gaitanos, H. Grigorian, A. Ho, E. E. Kolomeitsev, M. C. Miller, G. Röpke, J. Trümper, D. N. Voskresensky, F. Weber, and H. H. Wolter, Phys. Rev. C **74**, 035802 (2006).

[23] J. M. Lattimer, C. J. Pethick, M. Prakash, and P. Haensel, Phys. Rev. Lett. **66**, 2701 (1991).

[24] B. G. Todd-Rutel and J. Piekarewicz, Phys. Rev. Lett. **95**, 122501 (2005).

[25] Z. H. Li, U. Lombardo, H.-J. Schulze, W. Zuo, L. W. Chen, and H. R. Ma, Phys. Rev. C **74**, 047304 (2006).

[26] E. N. E. van Dalen, C. Fuchs, and A. Faessler, Eur. Phys. J. A **31**, 29 (2007).

[27] J. M. Lattimer and M. Prakash, Phys. Rep. **442**, 109 (2007).

[28] N. Alam, B. K. Agrawal, J. N. De, S. K. Samaddar, and G. Colò, Phys. Rev. C **90**, 054317 (2014).

[29] N. H. Tan, D. T. Loan, D. T. Khoa, and J. Margueron, Phys. Rev. C **93**, 035806 (2016).

[30] A. Burrows and J. M. Lattimer, Astrophys. J. **307**, 178 (1986).

[31] J.-J. Lu, Z.-H. Li, G. F. Burgio, A. Figura, and H.-J. Schulze, Phys. Rev. C **100**, 054335 (2019).

[32] A. N. Antonov, D. N. Kadrev, M. K. Gaidarov, P. Sarriguren, and E. M. de Guerra, Phys. Rev. C **95**, 024314 (2017).

[33] B.-A. Li, L.-W. Chen, and C. M. Ko, Phys. Rep. **464**, 113 (2008).

[34] A. Astier *et al.*, Eur. Phys. J. A **50**, 2 (2014).

[35] J. Margueron, R. H. Casali, and F. Gulminelli, Phys. Rev. C **97**, 025805 (2018).

[36] M. Baldo, A. Polls, A. Rios, H.-J. Schulze, and I. Vidaña, Phys. Rev. C **86**, 064001 (2012).

[37] S. Gandolfi, J. Carlson, S. Reddy, A. W. Steiner, and R. B. Wiringa, Eur. Phys. J. A **50**, 10 (2014).

[38] K. Hebeler, J. M. Lattimer, C. J. Pethick, and A. Schwenk, Astrophys. J. **773**, 11 (2013).

[39] W. M. Seif, J. Phys. G **38**, 035102 (2011).

[40] J. M. Lattimer and F. D. Swesty, Nucl. Phys. A **535**, 331 (1991).

[41] M. Baldo, I. Bombaci, and G. F. Burgio, Astron. Astrophys. **328**, 274 (1997).

[42] P. R. Chowdhury, D. N. Basu, and C. Samanta, Phys. Rev. C **80**, 011305(R) (2009).

[43] W. M. Seif and D. N. Basu, Phys. Rev. C **89**, 028801 (2014).

[44] F. Douchin and P. Haensel, Astron. Astrophys. **380**, 151 (2001).

[45] F. Douchin, P. Haensel, and J. Meyer, Nucl. Phys. A **665**, 419 (2000).

[46] E. Chabanat, P. Bonche, P. Haensel, J. Meyer, and R. Schaeffer, Nucl. Phys. A **635**, 231 (1998).

[47] M. Brack, C. Guet, and H.-B. Håkansson, Phys. Rep. **123**, 275 (1985).

[48] P. Bonche, S. Levit, and D. Vautherin, Nucl. Phys. A **436**, 265 (1985).

[49] D. T. Loan, N. H. Tan, D. T. Khoa, and J. Margueron, Phys. Rev. C **83**, 065809 (2011).

[50] M. Brack and P. Quentin, Phys. Lett. B **52**, 159 (1974).

[51] A. Roggero, A. Mukherjee, and F. Pederiva, Phys. Rev. C **92**, 054303 (2015).

[52] E. Rrapaj, A. Roggero, and J. W. Holt, Phys. Rev. C **93**, 065801 (2016).

[53] B. M. Santos, M. Dutra, O. Lourenço, and A. Delfino, Phys. Rev. C **92**, 015210 (2015).

[54] C. C. Moustakidis, T. Gaitanos, C. Margaritis, and G. A. Lalazissis, Phys. Rev. C **95**, 059904 (2017).

[55] H. Nakada, Phys. Rev. C **92**, 044307 (2015).

[56] D. T. Loan, B. M. Loc, and D. T. Khoa, Phys. Rev. C **92**, 034304 (2015).

[57] W. M. Seif, J. Phys. G **30**, 1231 (2004).

[58] D. T. Khoa, N. H. Phuc, D. T. Loan, and B. M. Loc, Phys. Rev. C **94**, 034612 (2016).

[59] M. V. Chushnyakova, R. Bhattacharya, and I. I. Gontchar, Phys. Rev. C **90**, 017603 (2014).

[60] M. Ismail and W. M. Seif, Phys. Rev. C **81**, 034607 (2010).

[61] W. M. Seif, Eur. Phys. J. A **38**, 85 (2008).

[62] D. Ni and Z. Ren, Phys. Rev. C **82**, 024311 (2010).

[63] G. Royer and H. F. Zhang, Phys. Rev. C **77**, 037602 (2008).

[64] W. M. Seif, A. M. H. Abdelhady, and A. Adel, Phys. Rev. C **101**, 064305 (2020).

[65] D. T. Khoa, W. Von Oertzen, and A. A. Ogloblin, Nucl. Phys. A **602**, 98 (1996).

[66] S. Mukhopadhyay, J. Lahiri, D. Atta, K. Imam, and D. N. Basu, Phys. Rev. C **97**, 065804 (2018).

[67] D. Atta and D. N. Basu, Phys. Rev. C **90**, 035802 (2014).

[68] S. A. Shapiro and S. L. Teukolsky, Black Holes, *White Dwarfs and Neutron Stars: The Physics of Compact Objects* (John Sons & Wiley, New York, 2008).

[69] I. Bombaci, *Isospin Physics in Heavy Ion Collisions at Intermediate Energies* (Nova Science, New York, 2001).

[70] D. T. Khoa, G. R. Satchler, and W. von Oertzen, Phys. Rev. C **56**, 954 (1997).

[71] D. T. Khoa, W. vonOertzen, H. G. Bohlen, G. Bartnitzky, H. Clement, Y. Sugiyama, B. Gebauer, A. N. Ostrowski, T. Wilpert, M. Wilpert, and C. Langner, Phys. Rev. Lett. **74**, 34 (1995).

[72] D. T. Khoa and W. V. Oertzen, Phys. Lett. B **342**, 6 (1995).

[73] N. Anantaraman, H. Toki, and G. F. Bertsch, Nucl. Phys. A **398**, 269 (1983).

[74] W. M. Seif, A. S. Hashem, and R. N. Hassanien, Nucl. Phys. A **1008**, 122142 (2021).

[75] G. R. Satchler and W. G. Love, Phys. Rep. **55**, 183 (1979).

[76] W. M. Seif, Nucl. Phys. A **878**, 14 (2012).

[77] W. M. Seif, A. M. H. Abdelhady, and A. Adel, J. Phys. G **45**, 115101 (2018).

[78] D. T. Khoa and H. S. Than, Phys. Rev. C **71**, 044601 (2005).

[79] D. T. Khoa, H. S. Than, and Do Cong Cuong, Phys. Rev. C **76**, 014603 (2007).

[80] J. P. Jeukenne, A. Lejeune, and C. Mahaux, Phys. Rev. C **16**, 80 (1977).

[81] W. Zuo, I. Bombaci, and U. Lombardo, Eur. Phys. J. A **50**, 12 (2014).

[82] C. Xu, B. A. Li, and L. W. Chen, Eur. Phys. J. A **50**, 21 (2014).

[83] A. Lejeune, Phys. Rev. C **21**, 1107 (1980).

[84] M. Golshanian, O. N. Ghodsi, R. Gharaei, and V. Zanganeh, Chin. Phys. Lett. **30**, 102502 (2013).

[85] N. D. Chien and D. T. Khoa, Phys. Rev. C **79**, 034314 (2009).

[86] Azza O. El-Shal, Phys. At. Nucl. **66**, 2117 (2003).

[87] D. T. Khoa and Do Cong Cuong, Phys. Lett. B **660**, 331 (2008).

[88] Le Hoang Chien, D. T. Khoa, Do Cong Cuong, and N. H. Phuc, Phys. Rev. C **98**, 064604 (2018).

[89] D. T. Loan, D. T. Khoa, and N. H. Phuc, J. Phys. G **47**, 035106 (2020).

[90] D. T. Khoa, Le Hoang Chien, Do Cong Cuong, and N. H. Phuc, Nucl. Sci. Tech. **29**, 183 (2018).

[91] N. M. Hugenholtz and L. Van Hove, Physica **24**, 363 (1958).

[92] M. Prakash, I. Bombaci, M. Prakash, P. J. Ellis, J. M. Lattimer, and R. Knorren, Phys. Rep. **280**, 1 (1997).

[93] A. W. Steiner, M. Prakash, J. M. Lattimer, and P. J. Ellis, Phys. Rep. **411**, 325 (2005).

[94] P. S. Koliogiannis and Ch. C. Moustakidis, Astrophys. J. **912**, 69 (2021).

[95] J. M. Lattimer, K. A. van Riper, M. Prakash, and M. Prakash, Astrophys. J. **425**, 802 (1994).

[96] J. M. Lattimer, Physics **11**, 42 (2018).

[97] S. Kubis, Phys. Rev. C **76**, 025801 (2007).

[98] A. D. Kaminker, C. J. Pethick, A. Y. Potekhin, V. Thorsson, and D. G. Yakovlev, Astron. Astrophys. **343**, 1009 (1999).

[99] N. K. Glendenning, *Compact Stars: Nuclear Physics, Particle Physics, and General Relativity* (Springer, New York, 2000).

[100] C. C. Moustakidis, T. Nikšić, G. A. Lalazissis, D. Vretenar, and P. Ring, Phys. Rev. C **81**, 065803 (2010).

[101] B.-J. Cai and L.-W. Chen, Phys. Rev. C **85**, 024302 (2012).

[102] T. R. Routray, X. Viñas, D. N. Basu, S. P. Pattnaik, M. Centelles, L. B. Robledo, and B. Behera, J. Phys. G **43**, 105101 (2016).

[103] C. Gonzalez-Boquera, M. Centelles, X. Viñas, and T. R. Routray, Phys. Rev. C **100**, 015806 (2019).